

Analytical and numerical study of coupled atomistic-continuum methods for fluids

Waiqing Ren

Courant Institute of Mathematical Sciences, New York University, New York, NY 10012, USA

Received 6 March 2007; received in revised form 5 July 2007; accepted 4 September 2007

Available online 20 September 2007

Abstract

The stability and convergence rate of coupled atomistic-continuum methods are studied analytically and numerically. These methods couple a continuum model with molecular dynamics through the exchange of boundary conditions in the continuum-particle overlapping region. Different coupling schemes, including velocity–velocity, flux–velocity, velocity–flux and flux–flux, are studied. It is found that the velocity–velocity and flux–velocity schemes are stable. The flux–flux scheme is weakly unstable. The stability of the velocity–flux scheme depends on the parameter T_c which is the length of the time interval between successive exchange of boundary conditions. It is stable when T_c is small and unstable when T_c is large. For steady-state problems, the flux–velocity scheme converges faster than the other coupling schemes.

© 2007 Elsevier Inc. All rights reserved.

Keywords: Coupled atomistic-continuum methods; Multiscale methods; Navier–Stokes equation; Molecular dynamics; Domain decomposition

1. Introduction

In recent years there has been a rapid growth of interest in modeling fluid systems which possess disparate length scales. These problems arise from, e.g. the development of micro- or nano-scale devices, the study of wetting phenomena on solid surface, the study of coalescence of liquid drops, etc. In most cases the difficulty arises from the complex interactions or chemical reactions in localized regions, which are often on atomistic scale, near the fluid–fluid or fluid–solid interface. In this situation, it is natural to decompose the physical domain of interest into the union of a localized region where the details of atomistic interaction are important and have to be modeled at the atomistic scale, and a larger region which can be modeled by continuum hydrodynamics. We will refer to these regions as the continuum region (or *c*-region) and the particle region (or *p*-region), respectively. In principle, multiscale methods of this type should have both the efficiency of the continuum model and the accuracy of the molecular model when necessary.

E-mail address: weiqing@cims.nyu.edu

In this domain-decomposition (DD) type of multiscale methods, the continuum and atomistic descriptions are coupled through exchanging boundary conditions in the continuum-particle overlapping region: The boundary condition for the continuum model in the c -region is provided by the molecular model in the p -region, and vice versa (see Fig. 1). Here two fundamental issues have to be addressed. The first is what kind of boundary condition we should impose on each model. Typical choices are velocity and flux. The second question is how to impose a specified boundary condition on each model. While imposing boundary conditions on continuum dynamics is more or less straightforward, the imposition of boundary conditions on particle dynamics represents the major difficulty in non-equilibrium or inhomogeneous molecular simulations. In this paper, we shall focus on the first issue and study the accuracy and efficiency of different coupling schemes. We leave the second issue for future work.

Several DD type of multiscale methods have been proposed in recent years [1–8]. These methods differ from each other in one or both of the aspects mentioned above. Based on the information exchanged in the overlapping region, these methods can be divided into two classes: Refs. [1–6] use the strategy of exchanging velocity: The velocity from the continuum model is imposed on the particle dynamics in the overlapping region, and the particle dynamics provides the velocity boundary condition for the continuum model. In contrast, Refs. [7,8] use the strategy of exchanging fluxes, i.e. the fluxes of conserved quantities, including the mass flux, momentum flux and energy flux, are exchanged in the overlapping region. These methods are also different in the way that the velocity or flux boundary conditions are imposed on the p -region. For example, in Ref. [1], the authors used a relaxational dynamics at the boundary of the p -region to ensure that the average particle velocity relaxes to the local continuum value. In Refs. [2,3], the velocity condition was imposed by using a Maxwellian demon: The velocity of particles near the boundary is randomly drawn from a Maxwellian distribution whose mean value is given by the continuum description. In Ref. [4], the desired average velocity at the boundary of the p -region was achieved by using a particle velocity transformation. Ref. [5] suggested to use a constrained particle dynamics, which is based on the Gauss principle of least constraint, to achieve the desired average velocity in the overlapping region. In the more recent work of Werder et al [6], the authors emphasized the point that the disturbance to the fluid structure should be minimal when imposing such boundary conditions. Their method includes several components: a specular wall at which the particles are reflected, an effective boundary potential, consistent body forces for imposing the mean velocity, and a particle insertion/removal algorithm. Refs. [7,8] proposed a methodology that couples compressible Navier–Stokes (NS) equation with molecular dynamics (MD) via flux exchanges. The mass, momentum and energy fluxes were imposed by inserting/removing particles, adding additional forces on particles near the boundary and as well as the use of Nosé-Hoover thermostats.

In the coupling scheme developed in Ref. [9], the particle dynamics is constrained by the velocity condition in the overlapping region, and it provides momentum flux as the boundary condition for the continuum model. This coupling scheme was designed using the principle of the heterogeneous multiscale method [10], and the projection method on the staggered grid was suggested as the macroscopic solver.

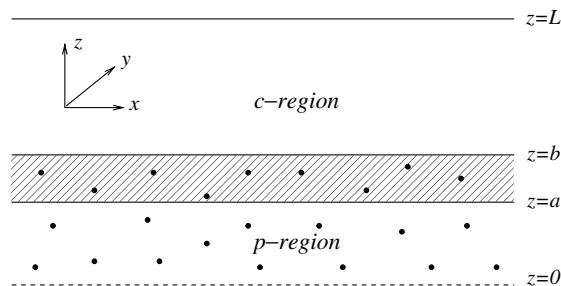


Fig. 1. Schematic of the coupled atomistic-continuum method. In the c -region between $z = a$ and $z = L$, the fluid is modeled by continuum hydrodynamics; in the p -region between $z = \pm b$, the fluid is modeled by MD. The c -region and p -region overlap between $z = a$ and $z = b$ (the shaded region). The two descriptions are coupled through exchanging boundary conditions at $z = a$ and $z = b$. The geometry is symmetric about $z = 0$, so only the upper half of the channel is shown here.

The DD type of multiscale methods considered here are different from classical DD methods for partial differential equations in at least two aspects. First, in classical DD methods continuum equations are used in all the sub-domains, while in the kind of DD methods considered here, one or more sub-domains are described by particle dynamics. As a consequence, the boundary conditions for the continuum dynamics have to be measured from the particle dynamics. These boundary conditions are inherently fluctuating and generally contains large statistical errors. Secondly, the sizes of the c -region and the p -region are often disparate: The c -region can be orders of magnitude larger than the p -regions. These two features have large effects on the accuracy and efficiency of the methods considered here.

In this paper, we will focus on two issues. The first is the stability of different coupling schemes. The main issue here is whether the statistical error introduced in the boundary conditions accumulates in the numerical solution. Secondly we will study the convergence rate of different schemes for steady-state problems. We will consider four types of coupling schemes: (1) velocity–velocity (VV); (2) flux–velocity (FV); (3) velocity–flux (VF) and (4) flux–flux (FF). Here the notation FV means that the continuum momentum flux is imposed on the particle dynamics, and the mean velocity is measured from the particle dynamics and imposed as the boundary condition on the continuum model, and similarly for the other three abbreviations. We will study the stability and convergence rate of these four coupling schemes using a system containing Lennard–Jones (LJ) particles in a channel. This is a simple problem. Nevertheless it contains all the essential components present in complex systems and thus is a good benchmark for the numerical schemes. Moreover, the simplicity of the problem allows us to understand the numerical results analytically, and thus helps us to gain insight into the coupling schemes.

The rest of the paper is organized as follows. In Section 2, we describe the system under study and present the algorithmic details of the four coupling schemes mentioned above. In Section 3, we apply these coupling schemes to the benchmark problem in which the system is in equilibrium. We will analyze the numerical results and study the effect of the statistical error on the numerical solutions. In Section 4, the coupling schemes are applied to an impulsively started shear flow. We compare the dynamics of the numerical solutions, and also study the convergence rate in steady-state calculations. Finally, we draw some conclusions in Section 5.

2. Problem setup and the coupling schemes

2.1. Setup of the problem

The system contains LJ particles in a channel. We will consider two situations. In the first situation the system is in equilibrium, and in the second one the system is sheared by constant motion of the two walls in opposite directions. A schematics of the decomposition of the channel is shown in Fig. 1. The geometry of the system and the decomposition of the channel are symmetric about the centerline of the channel, therefore for simplicity only the upper half of the channel is shown in the figure. The channel is decomposed into three regions: One p -region in the middle of the channel and two c -regions covering the rest of the channel. In the figure, the centerline of the channel is at $z = 0$, the p -region is between $z = \pm b$, and the upper c -region is between $z = a$ and $z = L$. The p -region and the c -region overlap in the region between $z = a$ and $z = b$. This region is called the overlapping region. The c -region is much larger than the p -region, i.e. $L \gg b$.

In the c -region, we model the system using the incompressible NS equation. The dynamics is homogeneous in the x and y directions, thus the NS equation reduces to

$$\rho \partial_t u - \partial_z \tau_{xz} = 0, \quad (1)$$

where τ_{xz} is the shear stress obeying the linear constitutive relation:

$$\tau_{xz} = \mu \partial_z u. \quad (2)$$

Here u is the x component of the fluid velocity, ρ and μ are the density and viscosity of the fluid, respectively. We use ∂_t and ∂_z to denote the derivatives with respect to the temporal variable t and the spatial variable z , respectively.

In the p -region, the system is modeled by MD in the three-dimensional space. Specifically we track the position and momentum of all constituting particles, which are governed by Newton's law:

$$\begin{cases} \dot{\mathbf{r}}_i = \mathbf{p}_i/m_i, \\ \dot{\mathbf{p}}_i = \mathbf{F}_i, \quad i = 1, 2, \dots, M, \end{cases} \tag{3}$$

where m_i , \mathbf{r}_i and \mathbf{p}_i are the mass, position and momentum of the i th particle, respectively, \mathbf{F}_i is the force experienced by the i th particle. Here we consider a simple situation where the particles interact via the pairwise LJ potential:

$$V(r) = 4\varepsilon \left(\left(\frac{\sigma}{r} \right)^{12} - \left(\frac{\sigma}{r} \right)^6 \right), \tag{4}$$

where r is the distance between particles, σ and ε are the characteristic length and energy of the particles. The atomistic force is given by $\mathbf{F}_i = -\sum_{j \neq i} \nabla V(r_{ij})$, where r_{ij} is the distance between the i th and j th particles.

The connection between the continuum model (1) and the particle dynamics (3) can be seen as follows. Let us define the empirical instantaneous momentum distribution:

$$\mathbf{m}^\omega(\mathbf{x}, t) = \sum_i \mathbf{p}_i(t) \delta(\mathbf{r}_i(t) - \mathbf{x}), \tag{5}$$

where $\delta(\mathbf{x})$ is the Dirac delta function. The superscript ω is used to emphasize that $\mathbf{m}^\omega(\mathbf{x}, t)$ is calculated from one configuration of the system. Momentum conservation for the particle dynamics can then be expressed as:

$$\partial_t \mathbf{m}^\omega + \nabla \cdot \boldsymbol{\tau}^\omega(\mathbf{x}, t) = 0, \tag{6}$$

where the momentum flux $\boldsymbol{\tau}^\omega(\mathbf{x}, t)$ is given by the following Irving–Kirkwood formula [15]:

$$\boldsymbol{\tau}^\omega(\mathbf{x}, t) = \sum_i \frac{1}{m_i} (\mathbf{p}_i \otimes \mathbf{p}_i) \delta(\mathbf{r}_i - \mathbf{x}) + \frac{1}{2} \sum_{j \neq i} ((\mathbf{r}_i - \mathbf{r}_j) \otimes \mathbf{F}_{ij}) \int_0^1 \delta(\lambda \mathbf{r}_i + (1 - \lambda) \mathbf{r}_j - \mathbf{x}) d\lambda, \tag{7}$$

where $\mathbf{F}_{ij} = -\nabla V(r_{ij})$ is the force acting on the i th particle by the j th particle. Ensemble averages of \mathbf{m}^ω and $\boldsymbol{\tau}^\omega$ give the macroscopic momentum and momentum flux.

Formula (7) expresses the momentum flux in terms of the microscopic variables. In the problem considered here, the mean particle velocity in the z direction (the transversal direction) is zero, therefore the xz component of the tensor in Eq. (7) gives the (negative of) shear stress. For LJ fluids, the linear constitutive relation as in Eq. (2) is a good approximation to the stress calculated directly from MD using formula (7), provided the shear rate is smaller than some critical value. This critical value depends on material parameters such as the fluid density, the temperature and etc. In the computation presented below, the shear rate in the whole channel is below the critical value, therefore the dynamics can be accurately described by the NS equation everywhere. We will use the solution of the NS equation as a benchmark for our multiscale method.

2.2. Macroscopic solver in the c -region

The c -region from $z = a$ to $z = L$ is covered by a mesh with N cells, as shown in Fig. 2. The mesh size is $h = (L - a)/N$. The grid points are denoted by $\{z_i = a + ih, i = 0, 1, \dots, N\}$. The velocity u is defined at $z_{i+1/2}$, the center of each cell. The shear stress τ_{xz} is defined at the grid points z_i and calculated using central difference:

$$(\tau_{xz})_i = \mu \frac{u_{i+1/2} - u_{i-1/2}}{h}. \tag{8}$$

Eq. (1) is then solved by the forward Euler method with the (macroscopic) time step Δt :

$$\rho \frac{u_{i+1/2}^{n+1} - u_{i+1/2}^n}{\Delta t} - \frac{(\tau_{xz})_{i+1}^n - (\tau_{xz})_i^n}{h} = 0. \tag{9}$$

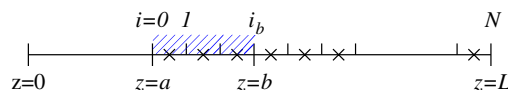


Fig. 2. Computational mesh in the c -region between $z = a$ and $z = L$. The velocity is defined at the center of each cell marked by crosses, and the shear stress is defined at the grid points. The shaded region between $z = a$ and $z = b$ is the overlapping region.

To solve the above equation, we need two boundary conditions: One at $z = a$ and one at the wall $z = L$. Here we use the no-slip condition at $z = L$, i.e. $u(L, t) = U$ where U is the velocity of the upper wall. The boundary condition at $z = a$ is provided by the particle dynamics in the p -region: The velocity $u_{1/2}$ at $z = z_{1/2}$ or the shear stress $(\tau_{xz})_0$ at $z = z_0$ is calculated from MD. Specifically, $u_{1/2}$ is calculated by averaging the particle velocities between $z = z_0$ and $z = z_1$ over some time interval. The length of the time interval is discussed at the end of this section. The shear stress $(\tau_{xz})_0$ is calculated using the Irving–Kirkwood formula (7). The formula is averaged over the region between $z = z_0 - h/2$ and $z = z_0 + h/2$ and also over some time interval which will be discussed later. Alternatively, one can calculate the shear stress by direct measuring the forces exerted on particles below $z = z_0$ by particles above $z = z_0$. The tangential component of this force per unit area gives the shear stress at $z = z_0$. The method based on the Irving–Kirkwood formula will be used in the numerical examples.

2.3. Microscopic solver in the p -region

In order to control the temperature of the system, we modify the Newton’s equation as follows. The y component of the particle velocity is coupled to a thermostat. This coupling is modeled by adding Langevin noise and friction terms to the dynamic equations [11]. The velocity Verlet algorithm is used to integrate the resulting equations with a (microscopic) time step δt . The LJ potential is truncated at a cutoff radius $r_c = 2.5\sigma$.

The MD calculation is done in 3d [13,14]. The simulation box has dimension $[0, L_x] \times [0, L_y] \times [-b, b]$. The values of the parameters are specified later. Boundary conditions are needed in order to fix the number of particles inside the box and also to match the particle dynamics with the continuum dynamics. The imposition of boundary conditions represents the major difficulty in the MD calculation. For the problem considered here, since the dynamics is homogeneous in x and y directions, we will use periodic boundary conditions in these two directions. In the z direction, we will use the reflection condition, i.e. the particle is reflected when it hits the boundaries at $z = \pm b$, and at the same time the z component of its velocity is reversed. To minimize the disturbance to the fluid structure caused by this artificial reflection of particles, we impose a boundary force on particles which are within the cutoff distance r_c from $z = \pm b$. Here we use the boundary force proposed by Werder et al [6]. This force, denoted by $f_n(r)$ where r is the distance to the boundary, is shown in Fig. 3 (the solid curve). Physically it is the averaged net force exerted on particles inside the box in the direction perpendicular to the boundary, from particles outside the box which are not included in the simulation. This force is precomputed from an equilibrium system with the same particle density and temperature as in the system considered here.

Next we see how to impose the velocity or shear stress condition at the boundary $z = b$ in order to match the particle dynamics with the continuum dynamics. Similar boundary conditions are imposed at $z = -b$. As shown in Fig. 2, $z = b$ is at one of the grid point in the mesh covering the c -region. We denote the index of this

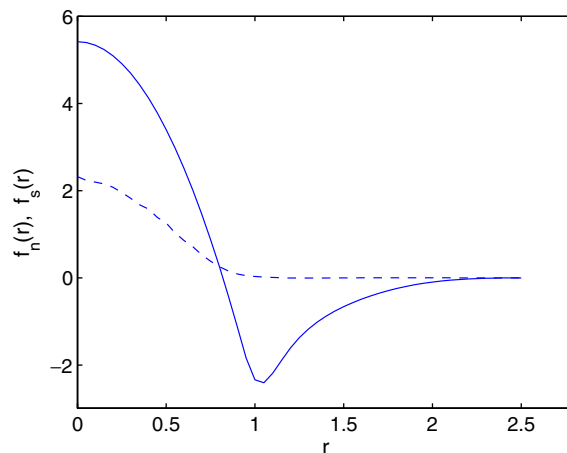


Fig. 3. The boundary force $f_n(r)$ (solid line) and the shear stress profile $f_s(r)$ (dashed line) used in MD.

grid point by i_b . By applying the velocity condition, we require the x component of the spatially averaged particle velocity between $z_{i_b-1} = b - h$ and $z_{i_b} = b$ to be equal to the continuum velocity $u_{i_b-1/2}$ in the corresponding i_b th cell (see Fig. 2). This constraint is enforced by adding a projection step to the standard velocity Verlet algorithm:

$$v_i^x = \tilde{v}_i^x - \frac{1}{N_b} \sum_j \tilde{v}_j^x + u_{i_b-1/2}. \quad (10)$$

Here \tilde{v}_i^x is the x component of the i th particle velocity after the velocity Verlet step. The sum is over particles between $z = b - h$ and $z = b$, and N_b is the number of particles in this region. Note that the above correction is imposed only on particles between $z = b - h$ and $z = b$.

To impose the shear stress $(\tau_{xz})_{i_b}$ on the particle dynamics, where $(\tau_{xz})_{i_b}$ is the shear stress calculated from the continuum model at $z = b$, we need to distribute this stress among particles near the boundary. This is done according to the profile $f_s(r)$ which is shown as the dashed curve in Fig. 3. Specifically, a particle with distance r from the boundary $z = b$ is exerted the force $(\tau_{xz})_{i_b} f_s(r)$ in the x direction. The profile $f_s(r)$, which is normalized according to $\rho \int_0^{r_c} f_s(r) dr = 1$, is obtained from a separate MD study of shear stresses at different shear rates. That study shows that the distribution of the microscopic shear stress obeys the universal profile $f_s(r)$, which is independent of the shear rate in the regime studied here.

2.4. Coupling procedure in the multiscale method

The dynamics in the c -region and p -region are coupled through exchanging velocity or shear stress in the overlapping region. As discussed earlier in the introduction, we shall in the following consider four coupling schemes: VV, FV, VF and FF. The coupling procedure is as follows. Starting from some initial condition, the continuum equation and MD are simultaneously solved in the c -region and p -region, with time steps Δt and δt , respectively. The boundary conditions at $z = \pm a$ for the continuum dynamics and at $z = \pm b$ for the particle dynamics are updated for every time interval T_c . In the following we will call the solution over each time interval T_c one iterate. The velocity or shear stress boundary conditions at $z = \pm a$ for the continuum dynamics in the $(n + 1)$ th iterate are calculated from the particle dynamics in the n th iterate, by averaging the particle velocities or the Irving–Kirkwood formula over the local cell with width h and over time interval T_c . Similarly the boundary conditions for MD at $z = \pm b$ at the $(n + 1)$ th iterate are provided by the continuum solution at the previous iterate.

In the numerical experiments presented in the next section, we choose the parameter T_c to range from the size of Δt to a value which is much larger than the hydrodynamic time scale. In the case when T_c is very large, the continuum and particle dynamics reach steady states at each iterate, and the above coupling procedure reduces to the Schwartz alternating method. This procedure is not suitable for dynamic problems, but might provide solutions for steady-state problems.

3. Results for the static problem

In the following, we will express all quantities in reduced atomic units: The unit of length is σ , the unit of time is $\sigma\sqrt{m/\varepsilon}$, the unit of density is m/ε^3 , the unit of temperature is ε/k_B where k_B is the Boltzmann constant, etc. As shown in Fig. 1, the size of the whole system, the p -region and c -region are determined by the parameters L , a and b . We will take $L = 101.2$, $a = 7.08$, and $b = 10.12$, respectively.

Recall that the geometry of the system and the decomposition of the computational domain are symmetric about $z = 0$, therefore the particle region is between $z = \pm b = \pm 10.12$. In the x and y directions, the MD box has the length $L_x = 40.01$ and $L_y = 7.74$, respectively. The particle density is 0.81. The temperature is 1.1. The pressure is 2.35. The time step in MD is $\delta t = 0.005$.

Consistent with the parameters in MD, the density ρ and the viscosity μ in the continuum equation (1) are 0.81 and 2.0, respectively. The viscosity is obtained from a MD simulation of a shear flow of the Lennard–Jones particles, where the ratio of the shear stress to the shear rate gives the viscosity. The continuum region

from $z = a$ to $z = L$ is discretized into a uniform mesh with grid size $h = 1.01$. The overlapping region between $z = a$ and $z = b$ covers three cells ($i_b = 3$, see Fig. 2). The time step used in solving Eq. (1) is $\Delta t = 0.15$.

In this section, we consider the problem where the system is in equilibrium. Therefore the exact solution is $u \equiv 0$. The numerical solutions calculated using the four coupling schemes are shown in Figs. 4–6. These figures correspond to different values of T_c : $T_c = m\Delta t$, where $m = 1, 10$ and 1.67×10^3 , respectively.

In the first calculation, the continuum and particle dynamics exchange boundary conditions at every continuum time step, i.e. $T_c = \Delta t = 30\delta t$. The velocity or flux boundary condition for the continuum model is averaged over 30 MD steps at each iterate. Fig. 4 shows the L_2 norm of the calculated velocity in the c -region as a function of time. This also shows the error of the numerical solution since the exact solution is identically equal to 0. The four panels in the figure correspond to the four coupling schemes: VV, FV, VF and FF from the top to the bottom, respectively. These figures have a common feature that the errors fluctuate with time. This fluctuation is induced by intrinsic statistical errors in the velocity or flux boundary conditions. The errors in the first three panels remain bounded with time, while in the last panel, which is the result of the flux–flux coupling scheme, the error exhibits a rather different behavior: It behaves like a random walk, and after 2×10^4 continuum time steps, it becomes ten times larger than the errors in the other three schemes.

Next we increased the time interval T_c to $10\Delta t$. We observed similar behavior for the numerical errors. The numerical results of the different coupling schemes are shown in Fig. 5.

Finally, we increased T_c to $1.67 \times 10^3 \Delta t$. This value is so large that the continuum and particle dynamics reached steady state at each iterate. The numerical results of the four coupling schemes are shown in Fig. 6. Note that the error of the VF scheme becomes very large after several iterations. The behaviors of the other

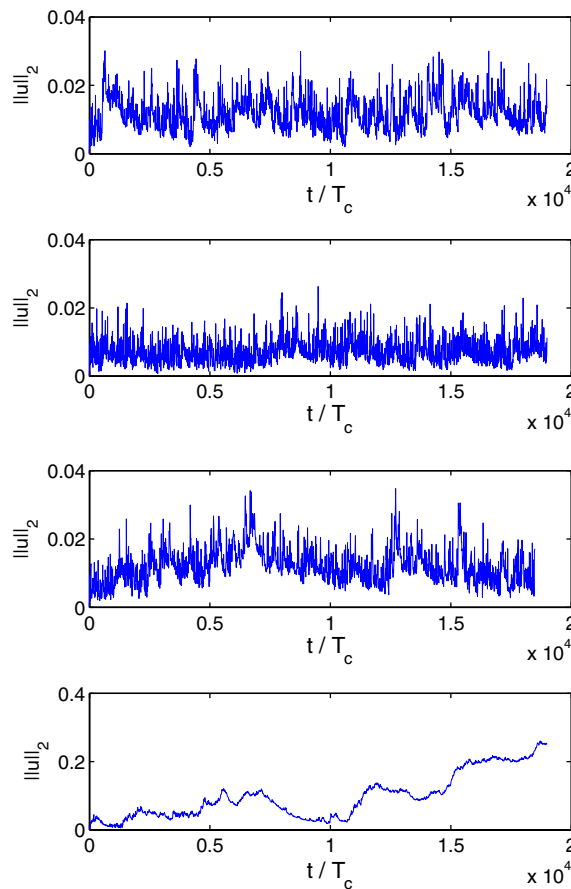


Fig. 4. Numerical results for the static problem. The figures show the L_2 norm of the numerical solution versus time (rescaled by T_c). Different curves correspond to different coupling schemes: VV, FV, VF and FF from the top to the bottom. The parameter $T_c = \Delta t$.

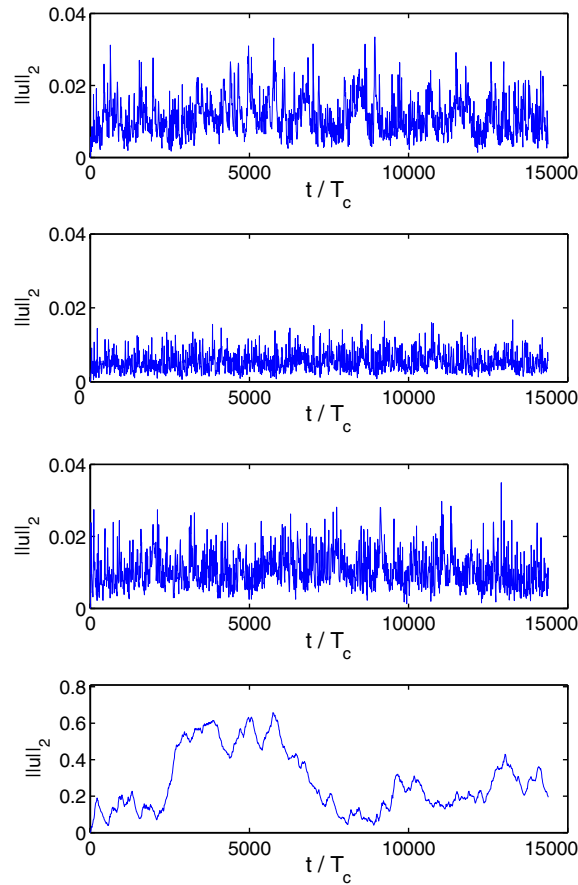


Fig. 5. Numerical results for the static problem. The figures show the L_2 norm of the numerical solution versus time (rescaled by T_c). Different curves correspond to different coupling schemes: VV, FV, VF and FF from the top to the bottom. The parameter $T_c = 10\Delta t$.

three schemes are similar as before: The errors in the VV and FV schemes remain bounded, while in the FF scheme the error behaves like a random walk. We also see that the errors of the VV and FV schemes are smaller than the errors in the previous two calculations with smaller T_c 's. This is due to the fact that the boundary conditions for the continuum model are averaged over longer time here and thus contain smaller statistical errors.

The difference in these numerical solutions is due to the different ways that the statistical errors are amplified or suppressed in the different coupling schemes. Next we look at the problem analytically.

3.1. Analysis of the problem for “ $T_c = +\infty$ ”

We first consider the case when T_c is large so that the system reaches steady state at each iteration. This corresponds to the numerical results shown in Fig. 6. In this case, the numerical solution of the different schemes can be written explicitly as follows:

Lemma 1. *The numerical solution of the static problem calculated using the VV, FV, VF and FF coupling schemes has the following form:*

$$u_n(z) = \left(\sum_{i=1}^n k^{n-i} \zeta_i \right) g(z), \tag{11}$$

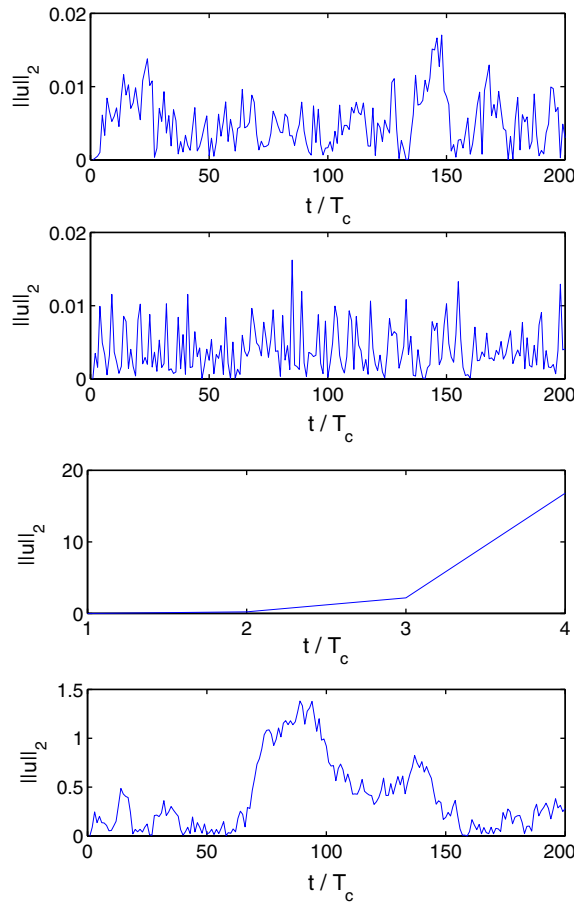


Fig. 6. Numerical results for the static problem. The figures show the L_2 norm of the numerical solution versus time (rescaled by T_c). Different curves correspond to different coupling schemes: VV, FV, VF and FF from the top to the bottom. The parameter $T_c = 1.67 \times 10^3 \Delta t$.

where $u_n(z)$ is the velocity at the n th iterate in the c -region. ξ_i is the statistical error introduced in the boundary condition at the i th iterate. The amplification factor k in the different schemes is given respectively by

$$k_{vv} = a(L - b)/(b(L - a)), \tag{12}$$

$$k_{fv} = a/(a - L), \tag{13}$$

$$k_{vf} = (b - L)/b, \tag{14}$$

$$k_{ff} = 1. \tag{15}$$

The function $g(z)$ in the different schemes is given respectively by

$$g_{vv}(z) = g_{fv}(z) = (L - z)/(L - a), \tag{16}$$

$$g_{vf}(z) = g_{ff}(z) = z - L. \tag{17}$$

The lemma can be proved by induction. Consider the VV coupling scheme for example. In the first iteration, an equilibrium MD is carried out in the p -region. The average velocity at $z = a$ is calculated and serves as the boundary condition for the continuum model in the upper c -region, and similarly for the lower c -region. Let us denote by ξ_1 the statistical error in this boundary condition. The steady state solution of the continuum equation (1) with the boundary condition $u(L) = 0$ and $u(a) = \xi_1$ is given by

$$u_1(z) = \xi_1 g_{vv}(z), \tag{18}$$

where $g_{vv}(z)$ is given in Eq. (16). Thus formula (11) is valid for $n = 1$. Assume the formula is valid for the n th iteration. In the $(n + 1)$ th iteration, the MD in the p -region is constrained so that the mean particle velocity is equal to $u_n(b)$ at $z = b$. Since the fluid is Newtonian the mean velocity in the p -region is then given by $v_{n+1}(z) = u_n(b)z/b$. The spatially and temporally averaged velocity at $z = a$ is

$$u_{n+1}(a) = v_{n+1}(a) + \xi_{n+1} = \sum_{i=1}^{n+1} k_{vv}^{n+1-i} \xi_i, \tag{19}$$

where ξ_{n+1} the statistical error of the averaged velocity, and k_{vv} is given by (12). With $u = u_{n+1}(a)$ at $z = a$ and the no-slip condition at $z = L$, the velocity in the c -region is then given by

$$u_{n+1}(z) = u_{n+1}(a)g_{vv}(z) = \left(\sum_{i=1}^{n+1} k_{vv}^{n+1-i} \xi_i \right) g_{vv}(z). \tag{20}$$

Therefore formula (11) is valid for the $(n + 1)$ th iteration. This proves the lemma for the VV coupling scheme. Following similar procedures, one can prove the lemma for the other three coupling schemes.

The amplification factor k_{vv} in (12) is less than 1 since $0 < a < b < L$. In the limit when the ratio $b/L \rightarrow 0$, k_{vv} becomes

$$k_{vv} = a/b = 1 - c/b, \tag{21}$$

where $c = b - a$ is the size of the overlapping region. Assume the statistical error ξ_i 's are independent identical random numbers with mean 0 and variance σ_v^2 , then it can be shown that the expectation of $\|u_n(z)\|_2$ is independent of n and satisfies

$$\langle \|u_n\|_2 \rangle \leq \left(\frac{1}{3(1 - k_{vv}^2)} \right)^{1/2} \sigma_v. \tag{22}$$

From (21) and (22) we see that the error of the numerical solution depends on the magnitude of the statistical error introduced in the velocity boundary condition, and also the size of the overlapping region relative to the size of the particle region. The fact that $k_{vv} < 1$ guarantees that the expectation of the numerical error is bounded. Thus the VV scheme is stable.

Similarly, one can show that in the FV scheme, the L_2 norm of the numerical solution in the c -region at the n th iterate also satisfies (22), but with k_{vv} replaced by k_{fv} and σ_v replaced by σ_f . Here k_{fv} is the amplification factor of the FV scheme given in Eq. (13), and σ_f^2 is the variance of the statistical error in the flux boundary condition. The absolute value of k_{fv} is smaller than 1, provided the c -region is larger than the p -region. This is always satisfied in practice. Therefore the FV scheme is also stable. Moreover, $|k_{fv}|$ is smaller than k_{vv} provided $L/b > 2$. This implies that under same conditions such as the same decomposition of the domain and the same sampling time, the FV scheme yields smaller error than the VV scheme. Note that here we only considered statistical errors in the measured boundary conditions, and we neglected other possible errors such as the error related to the imposition of boundary conditions on MD (e.g. imposing boundary conditions may change the fluid structure near the boundary, see Ref. [6]), the error in the viscosity and etc.

In the VF coupling scheme, the amplification factor $|k_{vf}| \gg 1$ since the size of the p -region is much smaller than the system size. As a result, the statistical error introduced at each iterate in the flux boundary condition is amplified geometrically in subsequent iterations, and this coupling scheme is unstable when T_c is large.

In the FF coupling scheme, the amplification factor k_{ff} is equal to 1. As a result, the slope of the numerical solution at the n th iterate is the superposition of the statistical errors introduced in previous iterations. This can be seen from Eq. (11). This explains the random walk like behavior of the numerical solution in the last panel of Fig. 6. We call this type of instability weakly unstable.

3.2. Analysis of the problem for finite T_c

We now turn our attention to study the stability of the different schemes when T_c is small compared to the hydrodynamic time scale, e.g. $T_c = \Delta t$ or $T_c = 10\Delta t$ as in the earlier calculations. In this case, the system does not necessarily reach steady state in each iteration.

The amplification factor as a function of T_c is calculated for each coupling scheme. The calculation is done as follows. We solve the continuum equation (1) in both the c -region and the p -region with the initial condition $u(z, 0) = v(z, 0) = 0$, and the boundary condition $u = 0$ at $z = \pm L$ for all t . Here $u(z, t)$ and $v(z, t)$ denote the velocity in the c -regions and in the p -region, respectively. The boundary conditions at $z = \pm a$ for the c -regions and at $z = \pm b$ for the p -region are as follows. In the first iteration, i.e. for $0 < t < T_c$, we use $u = 1$ as the boundary condition at $z = a$ for the upper c -region. This non-zero boundary condition mimics the statistical error introduced in coupled atomistic-continuum schemes. Similar boundary condition is imposed at $z = -a$ so that the solution is symmetric about the centerline of the channel. For the p -region, we use $v = 0$ at $z = \pm b$ in the first iteration. Therefore, for $0 < t < T_c$, the solution is $v \equiv 0$ in the p -region, and in the (upper) c -region the velocity solves:

$$\begin{cases} \rho \partial_t u - \mu \partial_z^2 u = 0 \\ u(z, 0) = 0, \\ u(a, t) = 1, \quad u(L, t) = 0 \quad \text{for } 0 < t < T_c. \end{cases} \tag{23}$$

In subsequent calculations, the boundary conditions at $z = \pm a$ for the c -regions and at $z = \pm b$ for the p -region are updated in each iteration: The boundary conditions at $z = \pm a$ in the $(n + 1)$ th iteration are provided by the solution of the p -region in the n th iteration, and similarly the boundary conditions at $z = \pm b$ are calculated from the solution in the c -regions. Therefore for $nT_c < t \leq (n + 1)T_c$ the boundary conditions at $z = \pm a$ and $z = \pm b$ are given respectively by

$$\begin{aligned} u(\pm a, t) &= v(\pm a, nT_c), \\ v(\pm b, t) &= u(\pm b, nT_c). \end{aligned} \tag{24}$$

There is no statistical error in these boundary conditions since we are using the continuum model in all the sub-domains. The coupling scheme is stable if the velocity field induced by the perturbation at $z = \pm a$ in the first iteration decays to zero in subsequent iterations, i.e. if the numerical solution converges to the exact solution $u \equiv 0$ as $n \rightarrow +\infty$; otherwise the scheme is unstable.

The L_2 norm of the numerical solution u is shown in Fig. 7 as a function of time. The parameter T_c is $10\Delta t$. The four curves correspond to the four coupling schemes (see the caption for details). These results show that the solution converges to $u \equiv 0$ as $n \rightarrow +\infty$ in the VV, FV and VF coupling schemes. In contrast, a finite error remains after convergence in the FF scheme. This is shown by the curve marked by circles. The magnitude of this error depends on the magnitude of the initial perturbation at $z = \pm a$, and also the value of the parameter T_c . This result suggests that in coupled atomistic-continuum methods, the statistical errors introduced in each iteration accumulate in the numerical solution, if the continuum and atomistic models are coupled through exchanging fluxes. This is consistent with the numerical result shown in Fig. 5.

The results in Fig. 7 also show that, after a short time, the solution of each scheme behaves as $\|u(\cdot, t)\|_2 \sim k^n$, where $n = t/T_c$ is the iteration number, and k is the amplification factor. The amplification factor can be determined by the slope of the curves in Fig. 7: $\log k = \lim_{n \rightarrow \infty} n^{-1} \log \|u(\cdot, t)\|_2$. It is equal to 1 in the FF scheme, and smaller than 1 in the other three schemes. Therefore, for the choice of $T_c = 10\Delta t$, the VV, FV and VF schemes are stable and the FF scheme is weakly unstable. The slopes of the curves in Fig. 7, thus the magnification factors, do not depend on the magnitude of the initial perturbation of the boundary condition at $z = \pm a$.

The amplification factor k depends on the parameter T_c . We carried out similar studies for different values of T_c and calculated the corresponding k . The result is shown in Fig. 8. The four curves in the figure correspond to the four schemes: VV (squares), FV (diamonds), VF (triangles) and FF (circles). As $T_c \rightarrow +\infty$, the factor k in these schemes converges respectively to the (absolute) value of k_{vv} , k_{fv} , k_{vf} and k_{ff} given in (12)–(15). The two curves in the upper panel of Fig. 8 corresponding to the VV and FV schemes are below $k = 1$ for all T_c :

$$k_{fv}(T_c) < k_{vv}(T_c) < 1. \tag{25}$$

Therefore these two schemes are stable for any choice of T_c . Furthermore, the fact that $k_{fv}(T_c) < k_{vv}(T_c)$ implies the statistical errors are suppressed faster in the FV scheme than in the VV scheme. Consequently the FV

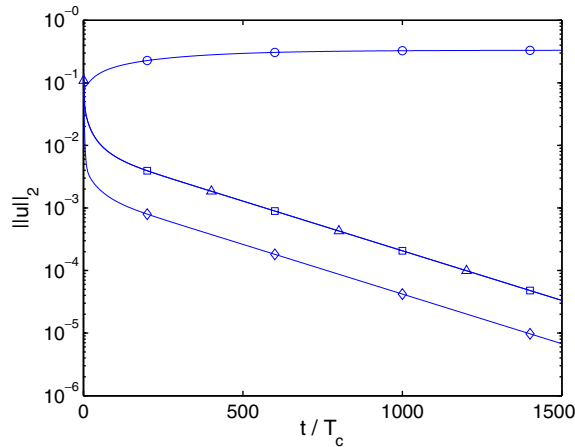


Fig. 7. Response of the system to an initial perturbation in the boundary condition. Different curves correspond to different schemes: VV (squares), FV (diamonds), VF (triangles), and FF (circles). The velocity decays to zero in the first three schemes; while a finite error remains in the FF scheme after convergence. The parameter $T_c = 10\Delta t$.

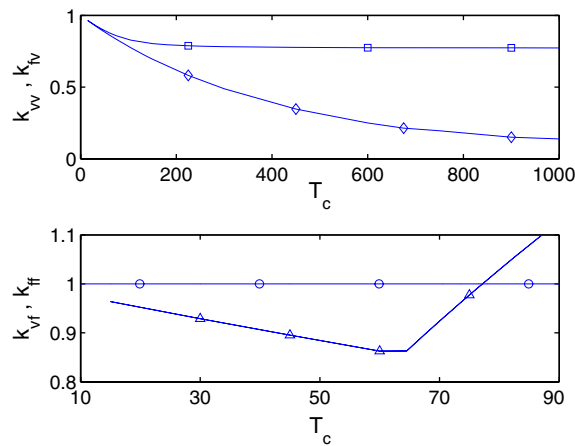


Fig. 8. The amplification factor k versus T_c for the four schemes: VV (squares), FV (diamonds), VF (triangles) and FF (circles).

scheme yields more accurate result. From the lower panel of Fig. 8, we see that there exists a critical value of T_c , below which the amplification factor of the VF scheme is smaller than 1. In this regime, the VF coupling scheme is stable. In the regime where k_{vf} is larger than 1, the statistical error will be amplified geometrically fast and the VF scheme becomes unstable. The FF scheme is weakly unstable for all T_c , since $k_{ff}(T_c) \equiv 1$. These analysis are consistent with the numerical results in Figs. 4–6.

From the numerical and analytical studies presented above, we arrive at the following conclusions regarding the stability of the four coupling schemes:

- (1) The VV and FV schemes are stable;
- (2) The VF scheme is stable when T_c is smaller than some critical value, and unstable otherwise;
- (3) The FF scheme is weakly unstable for any T_c .

4. Results for a dynamic problem

Next we consider the dynamics of an impulsively started shear flow. The set-up of the system is the same as before: It contains Lennard–Jones particles in a channel. The system is at rest initially. For $t > 0$ the two walls of the channel are sheared at constant speed $U = 5$ in opposite ($\pm x$) directions. The decomposition of the channel and the parameters such as the density, viscosity and the temperature, as well as the time steps remain the same as before. In the coupling schemes, the boundary conditions are exchanged between the c -region and the p -region at each continuum time step, i.e. $T_c = \Delta t = 0.15$.

The dynamics of the system calculated using the VV, FV, VF and FF schemes are shown in Figs. 9–12, respectively. The four panels in each figure show the numerical solution at $t = 360, 540, 870$ and $t = 3000$ (from the top to the bottom), respectively. These results are compared with the reference solution, which is obtained by solving the continuum Eq. (1) in the whole channel, with the initial condition $u = 0$ and the boundary condition $u(\pm L, t) = \pm U$ for $t > 0$. This reference solution is shown as the dashed curve in each panel. The solid curves are the numerical solutions of the different coupling schemes. Specifically, the oscillatory solid curve between $z = \pm 10$ in each panel is the numerical solution in the p -region, which was averaged over the period T_c which contains 30 MD steps. The smooth solid curve in the region $z \geq 7$ is the solution in the upper c -region. From these results we see that the numerical solutions obtained using the VV, FV and VF schemes agree well with the reference solution, and each resolves the dynamics. In contrary, the FF scheme fails as shown in Fig. 12.

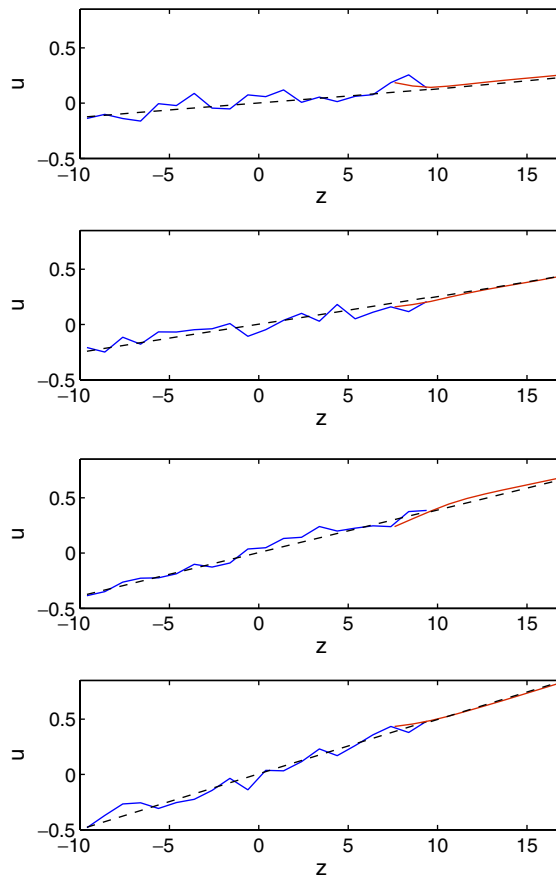


Fig. 9. Numerical solution of the impulsively started shear flow, obtained using the VV scheme. The four panels from the top to the bottom show the solution at $t = 360, 540, 870$ and 3000 , respectively. The dashed curve in each panel is the reference solution. The oscillatory curve between $z = \pm 10$ is the numerical solution in the p -region; the smooth solid curve in the region $z > 7$ is the numerical solution in the c -region.

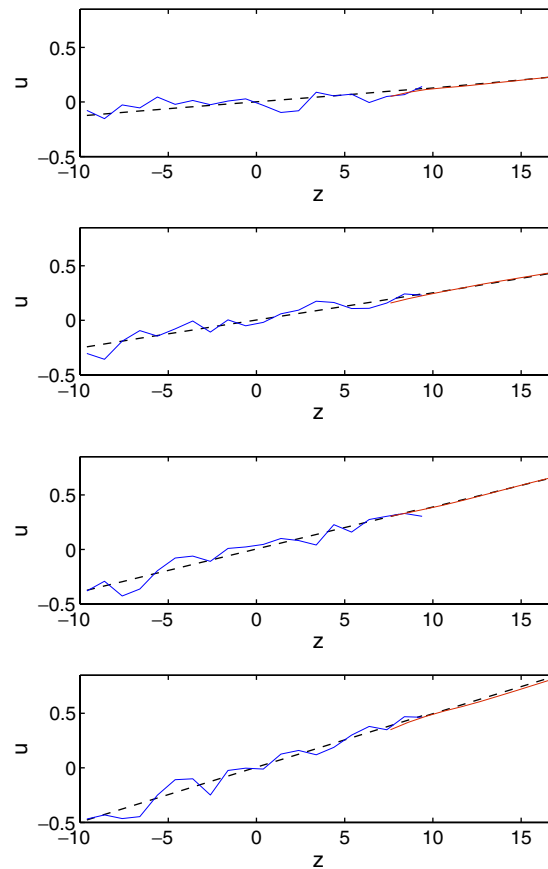


Fig. 10. Numerical solution of the impulsively started shear flow, obtained using the FV scheme (see the caption of Fig. 9 for details).

In Ref. [7], the authors solved a similar problem using the FF scheme. The coupling scheme was very successful in their calculation: The numerical solution at the steady state agrees with the expected Couette profile. There are several differences between their calculation and ours: First, in Ref. [7], the two walls of the channel were sheared with gradually increasing speed until the steady state value, while we considered an impulsively started shear flow. Secondly, the grid size (thus the region over which the shear stress was averaged) and the continuum time step in [7] are much larger than ours. They used a grid size $h = 7.6$ and an macroscopic time step Δt which was 100 times bigger than the MD time step, while in our calculation, $h = 1.01$ and Δt is 30 times of the MD time step. Consequently their measured stress boundary condition contained less statistical errors than ours. Finally, different MD thermostats were used in these two calculations. In Ref. [7], the MD were thermalized by applying a Langevin force on particles in the region where the continuum flux were imposed. The Langevin force contains a term involving the continuum velocity, which may penalize the discontinuity of the velocity across the overlapping region. In our calculation, the temperature of the MD system is controlled by a Langevin dynamics in the y direction only (perpendicular to the flow). These differences are possible causes of the discrepancy in the numerical results.

Next we study the convergence rate of the four schemes in the calculation of steady-state solutions. We increase T_c to $8000\Delta t$. This value is so large that the system reaches steady state in all sub-domains in each iteration. As explained earlier, the VF scheme is unstable in this case since the amplification factor $k > 1$. The FF scheme fails to converge to the Couette profile even in the absence of statistical errors. Indeed, the scheme converges after one iteration, and the converged solution is a stepwise function: It is $-U$ in the lower c -region for $z \leq -a$, U in the upper c -region for $z \geq a$, and 0 in the p -region. In contrast, the VV and FV schemes performed well for this problem. The numerical solutions of both schemes converged to the correct

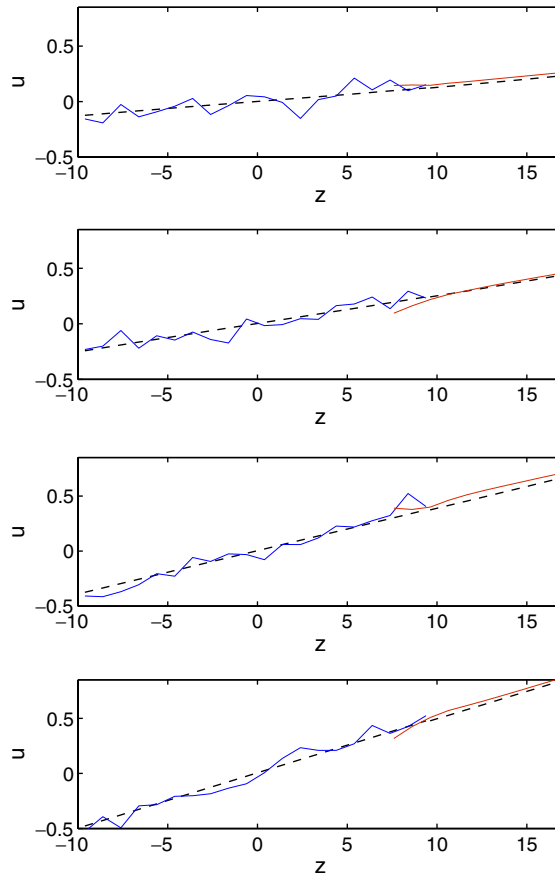


Fig. 11. Numerical solution of the impulsively started shear flow, obtained using the VF scheme (see the caption of Fig. 9 for details).

Couette profile $u_\infty(z) = Uz/L$ within the error bar. In Fig. 13, we plot the convergence history of these two schemes. Specifically, this figure shows the error $\|u_n - u_\infty\|_2$ versus the iteration number n . Here $u_n(z)$ is the numerical solution in the c -region at the n th iterate. The curve marked by squares corresponds to the VV scheme, and the curve marked by diamonds corresponds to the FV scheme. From these results, we see that the FV scheme converges much faster than the VV scheme. The FV scheme converges to the steady-state solution within the error bar in only two iterations, while the VV scheme takes 17 iterations. The convergence rates of these two schemes are also determined the amplification factor k : The smaller the factor, the faster the convergence, and vice versa. For the system considered here, the amplification factor of the FV scheme is $k_{fv} = 0.08$, and the amplification factor of the VV scheme is $k_{vv} = 0.7$. Therefore the FV scheme has a faster convergence rate.

Finally we study how the size of the overlapping region affects the convergence rate. In the following calculation, the p -region remains unchanged and covers the region between $z = \pm b = \pm 10.12$. The c -regions become smaller so that the upper c -region now covers the region from $z = b - h$ to $z = L$ where $h = 1.01$ is the grid size, and similarly for the lower c -region. As a result, the overlapping region now contains only one cell. The VV scheme fails to converge in this case, since the velocity boundary condition is imposed and subsequently measured in the same cell. The FV scheme does not have this difficulty since it exchanges different information between the two models: It imposes the shear stress on MD and calculates the average particle velocity from MD in the overlapping cell. This is confirmed by the numerical results. The FV scheme converges in two steps to the Couette profile, which is shown as the dashed line marked with circles in Fig. 13.

We also applied the different coupling schemes to a Poiseuille problem. The system is the same as before. The flow is driven by an external force $f = 2 \times 10^{-3}$ in the x -direction. The continuum region is between

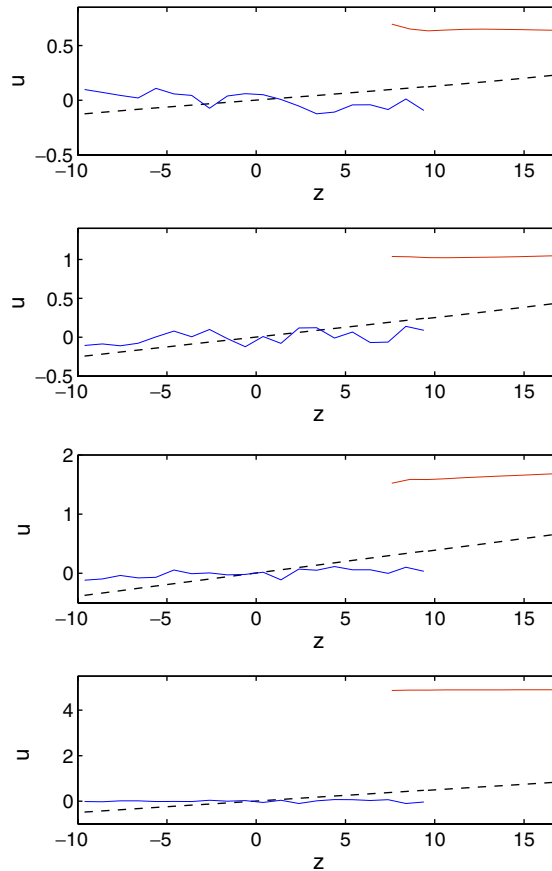


Fig. 12. Numerical solution of the impulsively started shear flow, obtained using the FF scheme (see the caption of Fig. 9 for details).

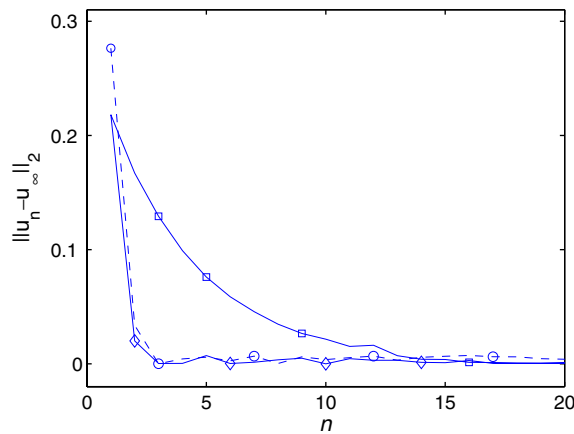


Fig. 13. Convergence history of the VV scheme and the FV scheme in the steady-state calculation of the impulsively started shear flow. The two solid curves marked by squares and diamonds correspond respectively to the VV scheme and the FV scheme, while the overlapping region contains three cells. The dashed curve marked by circles corresponds to the FV scheme where the overlapping region contains only one cell. The VV scheme fails to converge in this case.

$z = \pm 90.4$ (in the middle of the channel). The two particle regions are located at $-L < z < -87.1$ and $87.1 < z < L$, respectively (next to the two walls). In the MD calculation, each of the two solid walls is modeled by two layers of face-centered cubic lattice with density 1.86. Besides the inter-molecular forces, the fluid par-

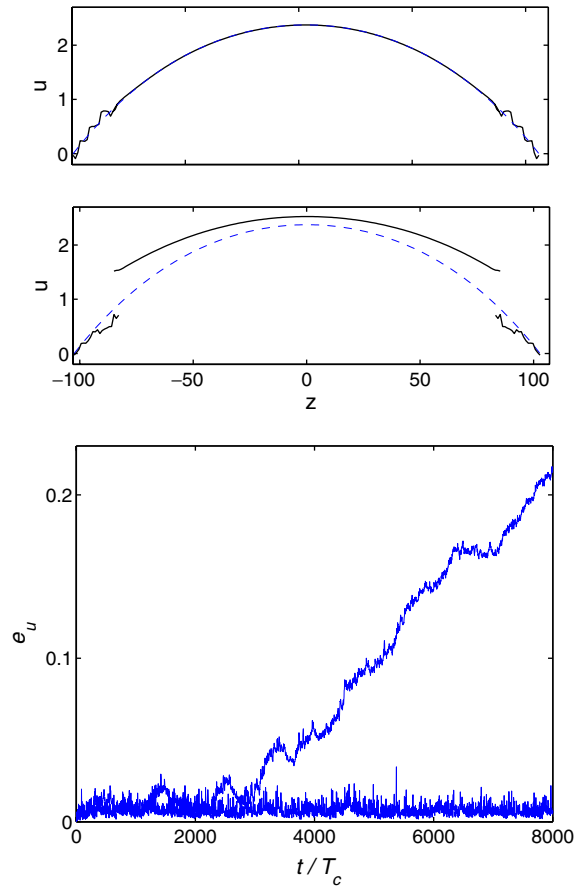


Fig. 14. Upper and middle panel: Numerical solution to the Poiseuille problem at $t = 1500$, obtained using the FV scheme (upper panel) and the FF scheme (middle panel), respectively. The dashed curve is the reference solution. The oscillatory curves at the two ends are the numerical solution in the p -region; the smooth curve in the middle is the numerical solution in the c -region. Lower panel: The error of the numerical solution versus time. The two curves correspond to the FV scheme (lower curve) and the FF scheme (upper curve), respectively.

ticles also feel the external force f . In the continuum region, the Eq. (1) with the additional term ρf on the right-hand side is solved. The grid size and the time step used in the discretization are the same as before. The fluid is at static initially. The continuum model and the MD exchange boundary conditions for every macro time step, i.e. $T_c = \Delta t$. The numerical results obtained by the different coupling schemes are shown in Fig. 14. In the upper and the middle panels, the solid curves are the numerical solution at $t = 1500$ obtained using the FV (upper panel) and the FF (middle panel) scheme, respectively. The dashed curves are the reference solution obtained by solving the continuum equation in the whole channel. Similar to the Couette flow, the velocity becomes discontinuous across the continuum-particle overlapping region in the FF scheme, and this discontinuity increases with time. In contrast, the numerical solution obtained using the FV scheme agrees well with the reference solution. This can also be seen from the lower panel which shows the error of the numerical solution as a function of time. The two curves correspond to the FF scheme (upper curve) and the FV scheme (lower curve), respectively. The error is defined as the L_2 -norm of the difference between the numerical solution and the reference solution. The other two schemes perform similarly to the FV scheme.

5. Conclusion

We have studied the stability and convergence rate of four coupling schemes: VV, FV, VF and FF. We found that the VV and FV coupling schemes performed well for both the static and dynamic problems. In

both schemes, the statistical error introduced in the boundary conditions in each iteration is suppressed exponentially fast with the iteration number n , and the error of the numerical solution remains bounded. The VF scheme performs similarly when the parameter T_c is below some critical value, but for large T_c , the statistical error is amplified geometrically fast with n and the scheme becomes unstable. The FF scheme is weakly unstable for any choice of T_c , in the sense that the statistical error accumulates in the numerical solution at a linear pace throughout the calculation. Therefore the FF scheme is not suitable for long time simulations. But for finite time calculations, one might still obtain reasonable solution provided the statistical error is small enough, as in the example in Ref. [7].

In this connection, let us mention the recent work of Delgado-Buscalioni and co-workers [12]. In this work, the authors proposed an improved version of the FF coupling scheme. This new scheme uses a mixed boundary condition for the continuum model. The boundary condition includes the momentum flux and also velocity, both of which are calculated from MD. This coupling scheme was proposed to improve the continuity of the numerical solution in the overlapping region. Our analysis suggests that it also help improving the stability and convergence of the original FF scheme.

In the setting of Schwartz alternating method, we studied the convergence rate of the VV and FV schemes for steady-state problems. We found that the FV scheme has much faster convergence rate than the VV scheme. This is mainly due to the disparate size of the continuum and particle regions. In the VV scheme, the convergence rate is determined by the size of the overlapping region relative to the p -region (see Eq. (21)), while in the FV scheme it is determined by the ratio of the p -region and the c -region. The convergence rate of the FV scheme is insensitive to the size of the overlapping region. This is confirmed by an numerical example in which the overlapping region is decreased to the minimal size which contains only one cell, and the FV coupling scheme performs equally well.

Overall, the FV coupling scheme performs the best for the aspects considered here. It has better accuracy and faster convergence rate. It should be noted that here we only considered the statistical error introduced in the boundary condition, and we left out other possible errors, e.g. the error related to the imposition of boundary conditions (including the boundary force, the velocity and fluxes) on particle dynamics. In particular, the methods used here and in the literature to impose these boundary conditions (e.g. Eq. (10)) emphasize on the mean values of these quantities, and the fluctuations are not taken into account. This introduces error to the particle dynamics. These issues will be investigated in future work.

Acknowledgments

The author is grateful to Weinan E for his constant support and stimulating discussions throughout this work. The author also thanks Bob Kohn, Eric Vanden-Eijnden and Olof Widlund for helpful discussions. The work is partially supported by NSF Grant DMS-0604382.

References

- [1] S.T. O'Connell, P.A. Thompson, Molecular dynamics-continuum hybrid computations: a tool for studying complex fluid flows, *Phys. Rev. E* 52 (1995) 5792.
- [2] N. Hadjiconstantinou, A.T. Patera, Heterogeneous atomistic-continuum representation for dense fluid systems, *Int. J. Modern Phys. C* 8 (1997) 967.
- [3] N. Hadjiconstantinou, Hybrid atomistic-continuum formulations and the moving contact-line problems, *J. Comp. Phys.* 154 (1999) 245.
- [4] J. Li, D. Liao, S. Yip, Nearly exact solution for coupled continuum/MD fluid simulation, *J. Computer-Aided Mater. Des.* 6 (1999) 95.
- [5] X. Nie, S. Chen, W. E, M.O. Robbins, A continuum and molecular dynamics hybrid method for micro- and nano-fluid flow, *J. Fluid Mech.* 500 (2004) 55.
- [6] T. Werder, J.H. Walther, P. Koumoutsakos, Hybrid atomistic-continuum method for the simulation of dense fluid flows, *J. Comp. Phys.* 205 (2005) 373.
- [7] E.G. Flekkoy, G. Wagner, J. Feder, Hybrid model for combined particle and continuum dynamics, *Europhys. Lett.* 52 (2000) 271.
- [8] R. Delgado-Buscalioni, P.V. Coveney, Continuum-particle hybrid coupling for mass, momentum, and energy transfers in insteady fluid flow, *Phys. Rev. E* 67 (2003) 046704.
- [9] W. Ren, W. E, Heterogeneous multiscale method for the modeling of complex fluids and micro-fluidics, *J. Comp. Phys.* 204 (2005) 1.
- [10] W. E, B. Engquist, The heterogeneous multi-scale methods, *Comm. Math. Sci.* 1 (2003) 87.

- [11] G.S. Grest, K. Kremer, Molecular dynamics simulation for polymers in the presence of a heat bath, *Phys. Rev. A* 33 (1986) 3628.
- [12] R. Delgado-Buscalioni, E.G. Flekkoy, P.V. Coveney, Fluctuations and continuity in particle-continuum hybrid simulations of unsteady flows based on flux-exchange, *Europhys. Lett.* 69 (2005) 959.
- [13] M.P. Allen, D.J. Tildesley, *Computer Simulation of Liquids*, Oxford, 1987.
- [14] D. Frenkel, B. Smit, *Understanding Molecular Simulation*, Academic Press, 2002.
- [15] J.H. Irving, J.G. Kirkwood, The statistical mechanical theory of transport processes IV, *J. Chem. Phys.* 18 (1950) 817.